JOURNAL OF MATERIALS SCIENCE 21 (1986) 97–102

The oxidation of electroless Ni–B and Ni–P coatings in air at 800 to 1000° C

W. J. TOMLINSON, G. R. WILSON
Department of Materials, Lanchester Polytechnic, Coventry CV1 5FB, UK

The oxidation of electroless Ni–B coatings in air at 800 to 1000° C has been determined by kinetic, X-ray diffraction, and microscopical methods. Some data have also been obtained on the oxidation of Ni–P coatings, the oxidation of nickel, and the effect of Na_2SO_4 on the oxidation process. All kinetics followed the parabolic oxidation law and the rate increased in the order spectrographically pure nickel, commercially pure nickel, Ni–B, and Ni–P, with the Ni–P oxidizing approximately 1000 times faster than the spectrographically pure nickel. Fine surface deposits of Na_2SO_4 greatly increase the oxidation rate of all materials except the Ni–P coatings which appear to be immune to hot-corrosion. The nature of the oxidation processes are discussed.

1. Introduction

Electroless nickel plating is the autocatalytic reduction of aqueous nickel ions on to a suitable substrate. Depending upon the nature of the reducing agent the coatings contain approximately 5 to 10% phosphorus or approximately 1% boron. The detailed crystal structure and microstructure are uncertain with the as-deposited structure being considered both as an amorphous-like structure [1] and as a supersaturated solid solution of phosphorus dissolved in fcc nickel with numerous stacking faults [2]. Whatever the exact nature of the deposit, the structure is unstable and at about 300° C transforms to a crystalline mixture of nickel and Ni_3P [3, 4]. At 11% P there is a eutectic mixture of nickel and Ni_3P with a melting point of 880° C. Ni–B deposits are much purer than the Ni–P deposits [5, 6]. Deposits formed by using dimethylamine borane as the reducing agent contain only 0.25% B and have a melting point of 1455° C [6]. The main reasons for the use of electroless deposits are the ease of plating, uniform deposit thickness, excellent corrosion resistance, and outstanding engineering properties of the deposit [7]. A major advantage of the autocatalytic nature of the process is that the deposit may be formed on non-conducting substrates and this, together with the physical properties of the deposit, has led to the use of such coatings in the electronics industry as thin film resistors [8–10].

Integrated circuit thick film technology requires the metal conductors to resist oxidation during firing [4]. Ni–P deposits start to oxidize above about 400° C [4], and above 800° C decomposition of phosphide and evaporation of phosphorus from the coating occurs [11]. Above 600° C migration of phosphorus to the surface and formation of P_2O_5 has been observed [12], and with Ni–P–B coatings many compounds including Ni_3B, NiO, and B_2O_3 are formed when the coating is heated in air [13]. A kinetic study at 800 to 1000° C showed that a Ni–P deposit oxidized about 100 times faster than pure nickel [14], and in a study aimed at reducing the amount of oxidation of Ni–P deposits it was found that B_2O_3 added to a Ni–P–glass mixture decreased the amount of oxidation [4].

It thus appears that the phosphorus in the Ni–P coating is the cause of the poor oxidation resistance of the alloy, and the much purer Ni–B coatings may be expected to have a much improved resistance to oxidation. The present work investigates the oxidation of electroless Ni–B deposits in air at 800 to 1000° C. For comparison the oxidation behaviour of a commercial nickel and an electroless Ni–P deposit are examined. The effect of a fine surface deposit of Na_2SO_4 is also briefly investigated.

2. Experimental details

Commercial electroless nickel coatings were deposited on machined mild steel coupons with a hole for a suspension wire. The Ni–B coatings were deposited from a dimethylamine borane bath and had a nominal composition 0.25% B. Two batches of Ni–B coatings were obtained, each batch from a different bath, on coupons 30 mm × 30 mm × 3 mm (first lot) and 10 mm × 10 mm × 2 mm (second lot). Microscopical examination showed the coatings to be of a uniform thickness 26 ± 2 μm and 12 ± 2 μm, respectively. A single lot of Ni–P coatings of nominal composition 10% phosphorus was formed on 30 mm × 30 mm × 3 mm coupons to a thickness of 26 ± 2 μm. Nickel of two levels of purity were used. Commercially pure nickel (Ni200) from H. Wiggins of nominal composition, wt %: C 0.15, Mn 0.35, Fe 0.4, S 0.01, Si 0.35, Cu 0.25, and boron and phosphorus each less than 40 ppm, were cut to 20 mm × 20 mm × 1 mm coupons, and spectrographically pure nickel (SPNi) from Johnson Matthey were cut to 10 mm × 10 mm × 1 mm coupons.

Analar quality Na_2SO_4 was applied to some specimens before oxidation as a uniform layer 0.5 ± 0.05 mg cm^{-2}. A fine deposit of Na_2SO_4 is used frequently as a severe test to assess the effect of small

0022–2461/86 $03.00 + .12

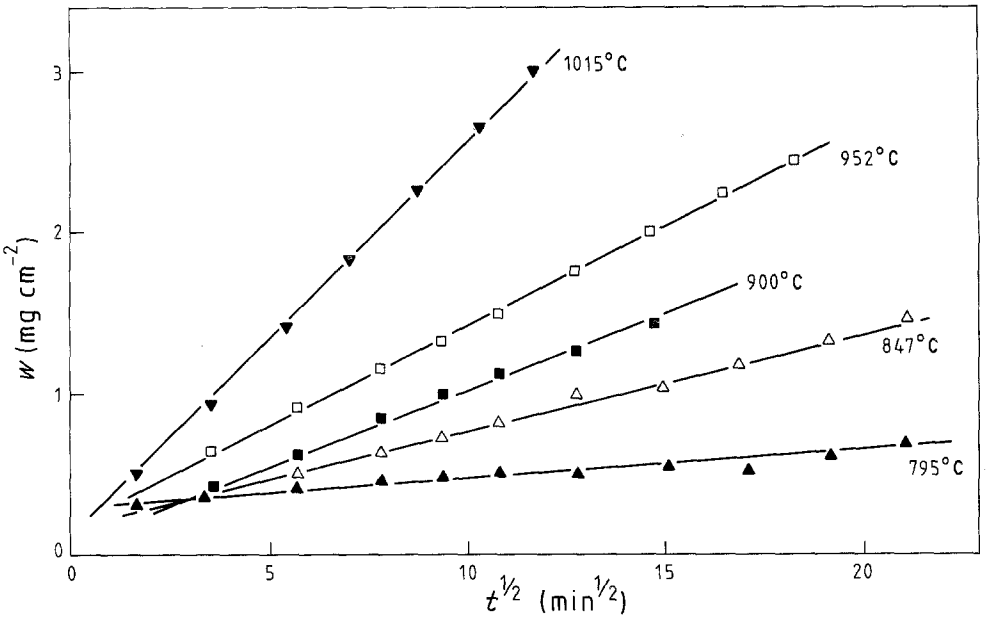

Figure 1 Parabolic kinetics for the oxidation of commercially pure nickel in air at 795 to 1015° C. Weight gain of oxygen as a function of time$^{1/2}$.

amounts of sulphur compounds on the oxidation process and consists of spraying specimens preheated to about 150° C with a saturated aqueous solution of Na_2SO_4. Evaporation of the water leaves a residue of Na_2SO_4 [15].

A Stanton thermogravimetric balance which could weigh to 0.25 mg and maintain the temperature to $\pm 2°$ C was used to determine the kinetics of oxidation. Before oxidation the specimen with a small suspension hook of Nichrome furnace wire was chemically cleaned in an aqueous solution of 8% H_2SO_4, 8% HNO_3, and 8% HCl, washed well in water and in alcohol and then air dried. The specimens were then transferred to the furnace pre-established at temperature. Oxidation was in static laboratory air.

Conventional X-ray diffraction (glancing angle of the surface oxide) and optical and scanning electron microscopy methods were used to examine the reaction products. Before metallographic examination the oxidized specimens were vacuum impregnated in a thermosetting resin.

3. Results

Kinetic data for the oxidation of Ni200, Ni–B and Ni–P coatings are expressed in parabolic form in Figs. 1 to 4. The parabolic oxidation law $w^2 = k_p t$, where w is the weight gain and t is time, is closely followed over the whole range of exposure conditions, and the associated Arrhenius function of the parabolic rate constant k_p, with the calculated activation energies (95% confidence level) are shown in Fig. 5 and Table I, respectively. It is clear that the rate of oxidation and the activation energy of oxidation both increase as the alloy content of the nickel increases. The effect of Na_2SO_4 on the oxidation process is shown in Fig. 6. It is seen that, except for the Ni–P coating, the effect of the Na_2SO_4 is to increase greatly the amount of oxidation and to change the form of the oxidation curve to being typically linear in the initial stage and protective in the later stage.

X-ray diffraction analysis was carried out in detail on the oxidized Ni–B coatings. Other specimens were examined on a limited and selective basis. The surface

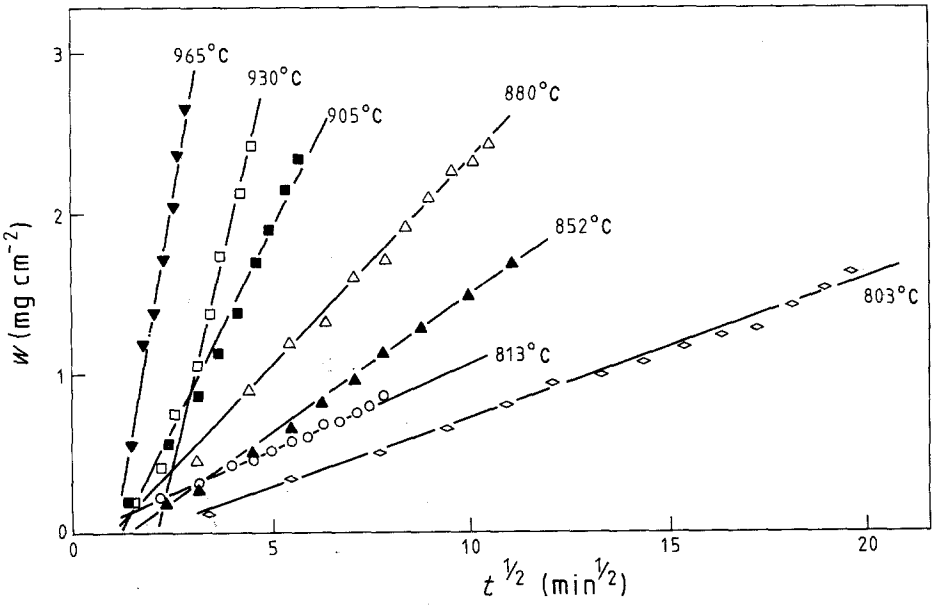

Figure 2 Parabolic kinetics for the oxidation of Ni–B(1) in air at 803 to 965° C. Weight gain of oxygen as a function of time$^{1/2}$.

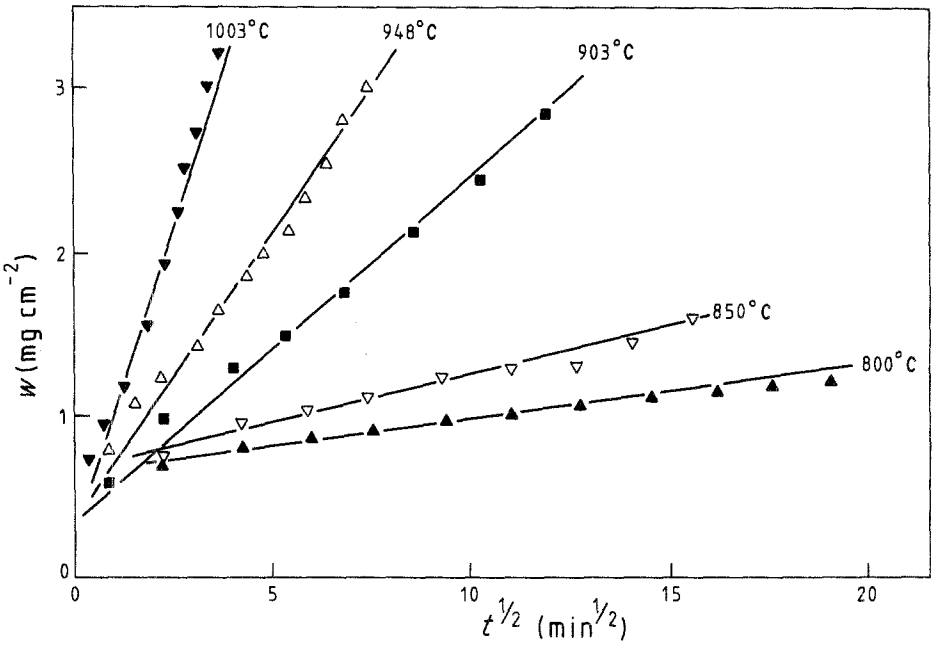

Figure 3 Parabolic kinetics for the oxidation of Ni–B(2) in air at 800 to 1003° C. Weight gain of oxygen as a function of time$^{1/2}$.

was examined (1) as-oxidized, and (2) after the surface oxide layer had been scraped away to detect the presence or otherwise of any interfacial compounds. On the Ni–B and Ni200 oxidized specimens only NiO was observed. With the Na_2SO_4-coated Ni–B no NiS was observed at the scale/metal interface. This contrasts with both the Ni200 and Ni–P cases where NiS was detected in the inner regions of the scale formed on the Na_2SO_4- coated specimens. A large number of compounds were observed on the oxidized Ni–P alloys. These include $(FeNi)_3P$ and P_2O_5 on its uncoated Ni–P specimens and $NaPO_4$, $FePS_3$, and $Na_3NiP_3O_{10}$ on the Na_2SO_4-coated specimens. In all cases, when a coating was oxidized to near destruction, Fe_3O_4 and Fe_2O_3 were observed but in no case was FeO detected.

Examination of the surface and cross-section by optical and scanning electron microscopy of the Ni–B coatings oxidized without Na_2SO_4 showed a relatively uniform and adherent scale. Only limited information was obtained on the effects of Na_2SO_4. Fig. 7a shows the very porous inner layer on the Na_2SO_4 coated Ni200, and Fig. 7b showed the bursting of the scale on a well-oxidized Na_2SO_4-coated Ni–B specimen. In both these cases the phenomena are associated with the accelerated oxidation induced by Na_2SO_4 (see Fig. 6). Figs. 7c and d show the surface scale on a Ni–P coating when uncoated and coated with Na_2SO_4, respectively. The uncoated scale is wrinkled (Fig. 7c) and the coated scale is compact (Fig. 7d). These effects appear to be related to the resistance of the Ni–P scale to accelerated oxidation by Na_2SO_4 (see Fig. 6). The separation of scale and substrate observed in Figs. 7c and d has occurred on cooling from the reaction temperature.

4. Discussion

It is clear from Figs. 1 to 4 that the parabolic oxidation law is followed by all specimens over the whole range of exposure conditions. In particular, there is no

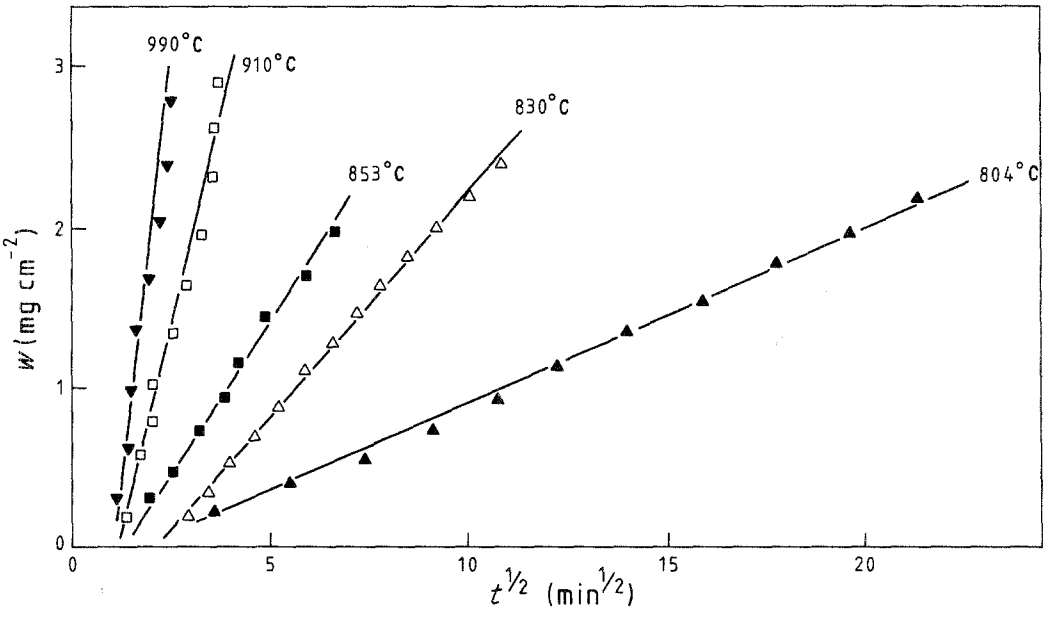

Figure 4 Parabolic kinetics for the oxidation of Ni–P in air at 804 to 990° C. Weight gain of oxygen as a function of time$^{1/2}$.

TABLE I Activation energies for parabolic oxidation

Material	$E_{ox}^{\ddagger}$ (kJ mol^{-1})
Spectrographically pure Ni	174 ± 14*
Ni200	206 ± 11
Ni–B(1)	306 ± 17
Ni–B(2)	325 ± 29
Ni–P	402 ± 46

*From [16].

indication of any change in the oxidation behaviour due to interdiffusion effects between the nickel coating and iron substrate. According to Hall [17], a 10 min heat-treatment at 870° C was calculated to form a nickel layer in iron about 2 μm thick and so for a maximum oxidation time of 100 min we calculate a penetration depth of $(x/2)^2 = 100/10$ i.e. $x = 6\,\mu$m. Allowing for the slightly faster diffusion rate of iron in nickel [17] it appears unlikely that much more than this will be affected by interdiffusion during a typical oxidation run. A 25 μm nickel coating reacts with 6 mg cm^{-2} oxygen to form NiO and so kinetic data should be unaffected by interdiffusion up to a weight gain of 4 mg cm^{-2}. The data in Figs. 2 to 4 are below 3 mg cm^{-2}, and even in the thinner 12 μm Ni–B(2) coatings (Fig. 3) there is no indication of non-parabolic oxidation behaviour. The parabolic rate constants depend greatly on the composition of the nickel. At 900° C, the parabolic rate constants for SPNi, Ni200, Ni–B(2), Ni–B(1), and Ni–P are 2.1×10^{-13}, 1.6×10^{-12}, 6.8×10^{-12}, 5.0×10^{-11}, and 1.8×10^{-10} g^2 cm^{-4} sec^{-1}, respectively. The difference in the Ni–B values will be discussed later.

Although there is an extensive literature on the oxidation of nickel there are many aspects of the process unresolved. Rosa [18] has recently summarized the main facts: nickel oxidizes according to a parabolic law in the temperature range of about 973 to 1100 K, only NiO forms, in air $Ni_{1-y}O$ is a p-type cation deficit semiconductor, the oxide grows by outward diffusion of Ni^{2+} via cation vacancies, and activation energies 174.4, 182.2, 188.5, 204.4, 204.8, 209.0, 213.2, 220.9, 280.1 and 285.4 kJ mol^{-1} have been determined for the process. In practice the oxidation process also involves the diffusion of oxygen inwards, probably by microcracks induced by growth stresses, and the outward diffusion of nickel along grain boundaries [19]. However, the principal transport mechanism above 800° C is the outward diffusion of nickel through the bulk lattice [19], and for the present purposes we consider only this process. In the present case, NiO was the only reaction product for the Ni200 and the Ni–B coating. The activation energy of 206 ± 11 kJ mol^{-1} for the oxidation of Ni200 is in good accord with the majority of values in the range of 204.4 to 220.9 kJ mol^{-1} and the oxidation process will consist of the outwards diffusion of Ni^{2+} via vacant cation sites. The values 306 ± 17 and 325 ± 29 kJ mol^{-1} obtained for NiB oxidation are well outside the range of values previously obtained and a different mechanism must be involved.

Using the notation of Kröger and Vink [20] the

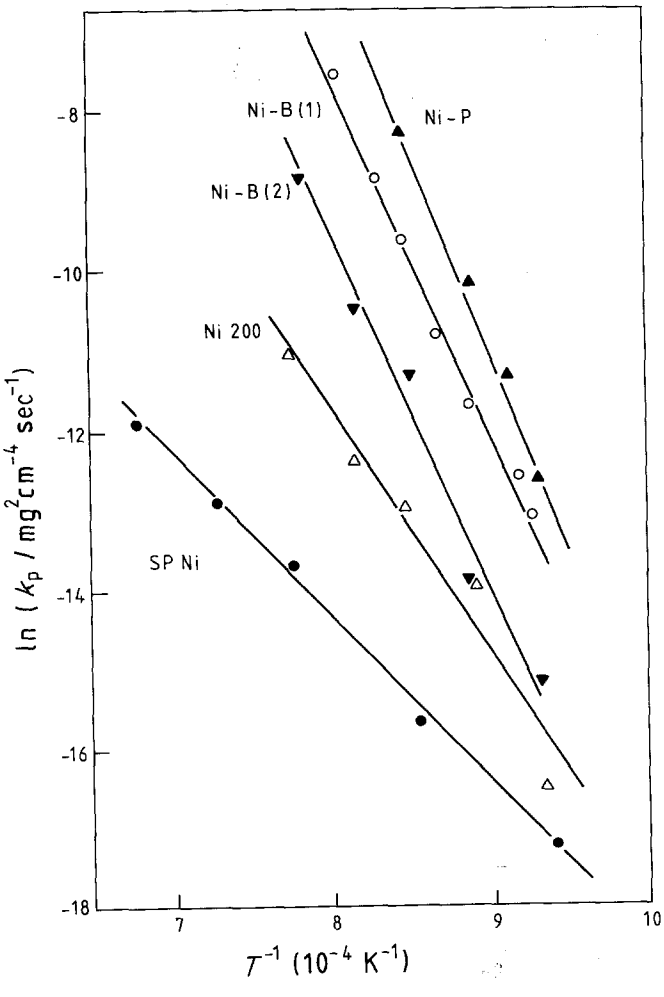

Figure 5 Arrhenius function of the parabolic oxidation rates. Data for the oxidation of spectrographically pure nickel air (SPNi; symbol ●) included from [16].

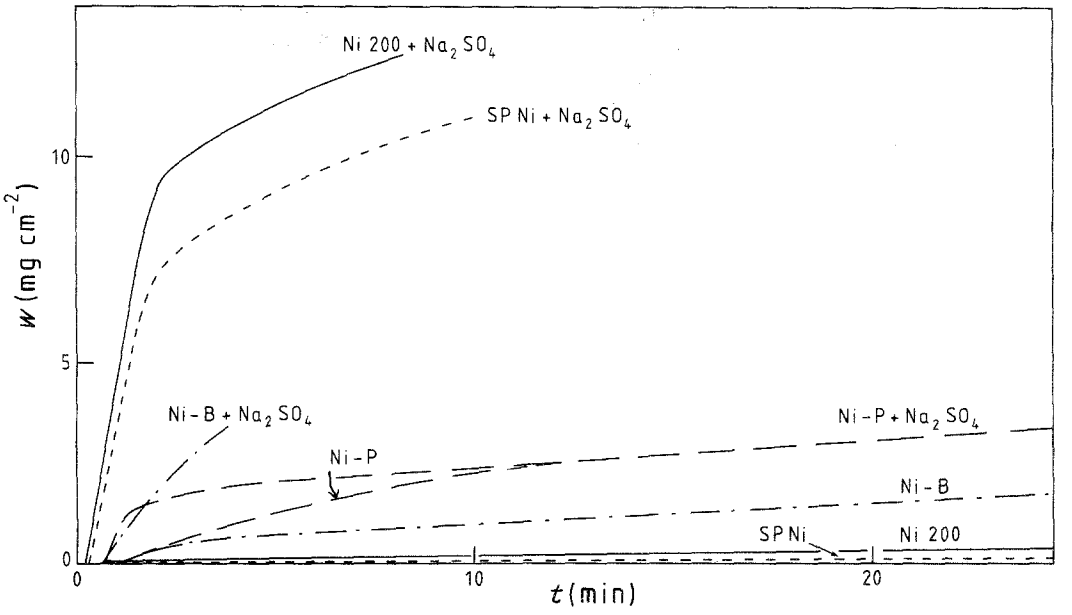

Figure 6 Oxidation kinetics of spectrographically pure nickel, Ni200, and Ni–B and Ni–P coatings in air at 900° C without and with a fine surface deposit of Na_2SO_4 (0.5 mg cm^{-2}). Weight gain of oxygen as a function time.

solution of O_2 in NiO to form singly ionized vacancies is

$$\tfrac{1}{2}O_{2(g)} = O_0^{\times} + V'_{Ni} + h^{\bullet}$$

the parabolic rate constant is related to the diffusion coefficients [21] by

$$k_p = 2D_{Ni} = 2D_{V'_{Ni}}[V'_{Ni}]_1 \ (m^2 \sec^{-1})$$

where $[V'_{Ni}]_1$ is the vacancy concentration at the O_2/NiO interface. During oxidation of Ni–B only NiO forms and if we assume that B^{3+} ions substitute on the nickel lattice sites then

$$B_2O_3 + h^{\bullet} = 3O_0^{\times} + 2B^{\bullet}_{Ni} + V'_{Ni}$$

The extent of nonstoichiometry in NiO is very small [21], e.g. y in $Ni_{1-y}O$ is about 5×10^{-3} at 1200° C, and we assume that the concentration of $B^{\bullet}_{Ni}$ provides more extensive vacancies than the intrinsic concentration. In this case [21]

$$k_p = \alpha D_{V'_{Ni}}[B^{\bullet}_{Ni}]$$

where α is a constant. On this basis we may interpret

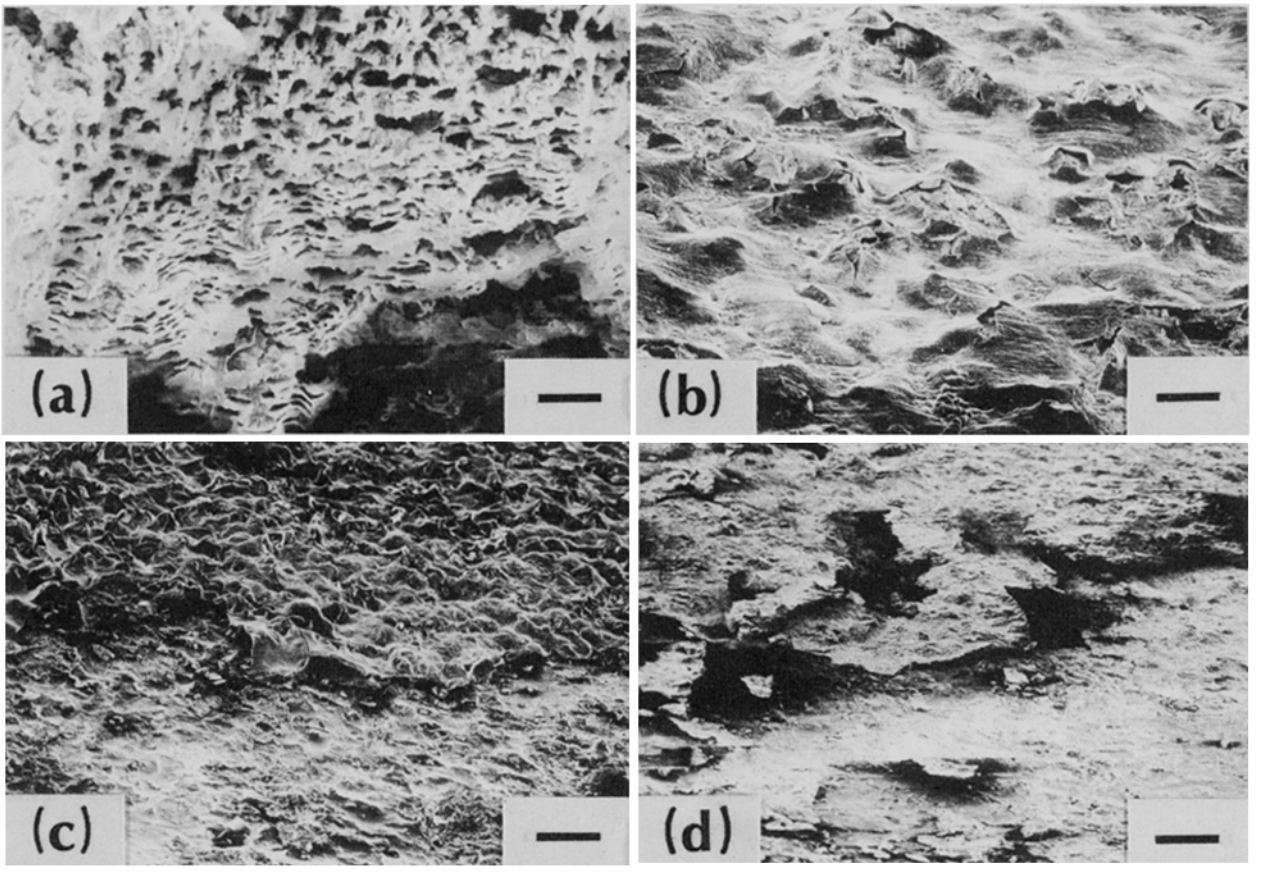

Figure 7 Microstructure of the oxidized layer formed at 900° C: (a) Ni200 with Na_2SO_4, (b) Ni–B with Na_2SO_4, (c) Ni–P without Na_2SO_4, (d) Ni–P with Na_2SO_4. Scale bars: (a) = 20 μm; (b, c, d) = 325 μm.

the present data. The higher oxidation rate of the Ni–B coatings is due to the increased concentration of extrinsic vacancies. The difference between the Ni–B(1) and Ni–B(2) rates is due to the different concentrations of boron in the two coatings. These were not analysed, but alloy electrodeposits and electroless coatings typically have substantial concentration differences owing to bath changes during deposition. The attractive Coulombic force between the negatively charged cation vacancy and positively charged boron ion will cause the two species to occupy adjacent cation sites [16, 22] as a defect complex $\{B^{\bullet}_{Ni} \cdot V'_{Ni}\}$. For extrinsic diffusion we may show that [16]

$$E^{*}_{oxn} \approx \Delta H^{*}_{oxn} = \Delta H^{*}$$

where ΔH^{*} is the enthalpy of vacancy motion in the doped NiO. Here, E^{*}_{oxn} is about $315\,kJ\,mol^{-1}$ and since the enthalpy of vacancy motion in pure NiO is about $103\,kJ\,mol^{-1}$ [23] then the extra $315 - 103 = 212\,kJ\,mol^{-1}$ of energy is needed to overcome the Coulombic attraction before the V'_{Ni} is free to diffuse.

The Ni–P coating had the highest oxidation rate. The activation energy of $402 \pm 46\,kJ\,mol^{-1}$ agrees with the value $377\,kJ\,mol^{-1}$ obtained previously [14]. Both NiO and P_2O_5 were present in the scale. In the $NiO–P_2O_5$ system [24] the compounds $Ni_3(PO_4)_2$, Ni_2PO_7, and $Ni(PO_3)_2$ with melting points 1350, 1395, and 1280° C, respectively, may form, but none of these were detected. The surface topography (Fig. 7d) suggests that the scale was molten at the reaction temperature and it appears that this is associated with the $Ni–Ni_3P$ eutectic. No detailed examination of the reaction products was carried out and the significance of the good parabolic plots (Fig. 4) and the high activation energy is not clear. Whilst the Ni–P coatings had the highest oxidation rate, they showed a remarkable resistance to Na_2SO_4 induced corrosion (Fig. 6).

Accelerated oxidation due to Na_2SO_4 is well known [25, 26]. In the linear region of SPNi, Ni200, and Ni–B oxidation (Fig. 6) the Na_2SO_4 has melted and the sulphate ion decomposed

$$SO_4^{2-} = \tfrac{1}{2}O_{2(g)} + SO_{2(g)} + O^{2-}$$

The O_2 and SO_2 are consumed in further oxidation and so the concentration of O^{2-} increases to maintain equilibrium. This dissolves the NiO scale to form nickelate ions by

$$2NiO + O^{2-} + \tfrac{1}{2}O_2 = 2NiO_2^{-}$$

in regions of high O^{2-}. The NiO_2^{-} diffuses to regions of low O^{2-} (the salt/gas interface region) and precipitates NiO. This results in a porous honeycomb scale (Fig. 7a) associated with the initial rapid oxidation period (Fig. 6). Eventually a dense NiO layer forms which makes the scale protective (Fig. 6) and this is associated with the formation of sulphide [25, 26]. This accounts for the absence of NiS at the metal/scale interface in the Ni–B alloys since the coating is so thin that the kinetics do not reach the protective oxide and NiS forming stage before all the Ni–B coating is consumed. The oxidation behaviour of the Na_4SO_4 coated Ni–P coatings is unusual in that no rapid oxidation occurs (Fig. 6). It seems that the Na_2SO_4 reacts preferentially with the phosphorus compounds to form solid $NaPO_4$, $FePS_3$, and $Na_3NiP_3O_{10}$ and these prevent operation of the normal rapid fluxing and oxidation of the scale. The protective scale formed with these compounds (Fig. 7d) is much more even and compact compared to the wrinkled surface of the Ni–P alloy oxidized without a Na_2SO_4 coating (Fig. 7c).

Acknowledgements

The authors wish to thank Shipley Chemicals for supply of the electroless nickel specimens, and R. Carey for the scanning electron microscope work.

References

1. J. DIXMER and K. DOI, *Compt. Rend.* **257** (1963) 2451.
2. A. H. GRAHAM, R. W. LINDWAY and H. J. READ, *J. Electrochem. Soc.* **112** (1965) 401.
3. L. F. SPENCER, *Metal. Finish* **72** (1974) 35, 50, 58; **73** (1975) 38.
4. I. BARYCKA, B. HOLODNIK and A. MISIUK, *Electrocomponent Sci. Tech.* **7** (1981) 221.
5. G. O. MALLORY, *Plating*, April (1971).
6. "Niposit 468 High Purity Electroless Nickel" (Shipley Chemicals, Humber Avenue, Coventry, UK) February, 1980.
7. S. S. TULSI, *Trans. Inst. Metal Finish.* **61** (1983) 147.
8. P. I. ÇOTE, *Sol. State Commun.* **18** (1976) 1311.
9. S. T. PAI and J. P. MARTON, *J. Appl. Phys.* **43** (1972) 282.
10. M. FERNÁNDEZ, J. M. MARTÍNEZ-DUART and J. M. ALBELLA, *Thin Solid Films* **112** (1984) L9.
11. M. V. KURTINAITENE, Yu. Yu. LYAUKONIS and I. I. ZHITKYAVICHUTE, *Liet. TSR Mokslu. Akad. Darbo B.* **123** (1981) 47; (*Metal Abst.* January (1982) 58-0063).
12. S. T. PAI and J. P. MARTON, *J. Electrochem. Soc.* **120** (1973) 1280.
13. F. R. FROLOVA, I. I. ZHITKYAVICHYUTE and I. K. GYANUTENE, *ibid.* **124** (1981) 41; (*Metal Abst.* February (1982) 11-0122).
14. W. J. TOMLINSON and S. C. RANDALL, *Corros. Sci.* **18** (1978) 573.
15. J. A. GOEBEL, F. S. PETTIT and G. W. GOWARD, *Met. Trans.* **4** (1973) 261.
16. W. J. TOMLINSON, *J. Chem. Soc. Far. I.* **73** (1977) 1334.
17. D. E. HALL, *J. Electrochem. Soc.* **129** (1982) 310.
18. C. J. ROSA, *Corros. Sci.* **22** (1982) 1081.
19. A. ATKINSON, R. I. TAYLOR and P. D. GOODE, *Oxid. Met.* **13** (1979) 519.
20. F. A. KRÖGER and H. J. VINK, "Solid State Physics", Vol. 5, edited by F. Seitz and D. Turnbull (Academic Press, London, 1955) pp. 431–5.
21. P. KOFSTAD, "Nonstoichiometry, Diffusion and Electrical Conductivity in Binary Metal Oxides" (Wiley-Interscience, New York, 1972) ch. 6 and 11.
22. R. A. PERKINS and R. A. RAPP, *Met. Trans.* **4** (1973) 193.
23. G. J. KOEL and P. J. GELLINGS, *Oxid. Met.* **5** (1972) 185.
24. J. F. SARVER, *Trans. J. Brit. Ceram. Soc.* **65** (1966) 191.
25. N. BIRKS and G. H. MEIER, "Introduction to High Temperature Oxidation of Metals" (Arnold, London, 1983) p. 146.
26. D. A. SHORES, in NACE 6, International Conference Series, "High Temperature Corrosion", edited by R. A. Rapp, Houston (1981) p. 493.

Received 24 July
and accepted 15 October 1984